Acta Pharmaceutica Sinica B 2025;15(4):2024−2038

Chinese Pharmaceutical Association
Institute of Materia Medica, Chinese Academy of Medical Sciences

Acta Pharmaceutica Sinica B

www.elsevier.com/locate/apsb
www.sciencedirect.com

ORIGINAL ARTICLE

Microbial metabolite 3-indolepropionic acid alleviated PD pathologies by decreasing enteric glia cell gliosis *via* suppressing IL-13Rα1 related signaling pathways

Meiyu Shang[a], Jingwen Ning[a], Caixia Zang[a], Jingwei Ma[a], Yang Yang[a], Zhirong Wan[b], Jing Zhao[b], Yueqi Jiang[a], Qiuzhu Chen[a], Yirong Dong[a], Jinrong Wang[a], Fangfang Li[a], Xiuqi Bao[a,*], Dan Zhang[a,*]

[a]*State Key Laboratory of Bioactive Substrate and Function of Natural Medicine, Institute of Materia Medica, Chinese Academy of Medical Sciences and Peking Union Medical College, Beijing 100050, China*
[b]*Department of Neurology, Aerospace Center Hospital, Beijing 100049, China*

Received 5 August 2024; received in revised form 11 September 2024; accepted 15 October 2024

KEY WORDS

Parkinson's disease;
Enteric glia cells;
3-Indolepropionic acid;
16S rRNA;
Pregnane X receptor;
IL-13Rα1;
Microbiota dysbiosis;
Inflammation

Abstract Although enteric glial cell (EGC) abnormal activation is reported to be involved in the pathogenesis of Parkinson's disease (PD), and inhibition of EGC gliosis alleviated gut and dopaminergic neuronal dysfunction was verified in our previous study, the potential role of gut microbiota on EGC function in PD still need to be addressed. In the present study, fecal microbiota transplantation revealed that EGC function was regulated by gut microbiota. By employing 16S rRNA and metabolomic analysis, we identified that 3-indolepropionic acid (IPA) was the most affected differential microbial metabolite that regulated EGC gliosis. The protective effects of IPA on PD were validated in rotenone-stimulated EGCs and rotenone (30 mg/kg i.g. for 4 weeks)-induced PD mice, as indicated by decreased inflammation, improved intestinal and brain barrier as well as dopaminergic neuronal function. Mechanistic study showed that IPA targeted pregnane X receptor (PXR) in EGCs, and inhibition of IL-13Rα1 involved cytokine−cytokine receptor interaction pathway, leading to inactivation of downstream JAK1−STAT6 pathway. Our data not only provided evidence that EGC gliosis was critical in spreading intestinal damage to brain, but also highlighted the potential role of microbial metabolite IPA in alleviating PD pathological damages through gut−brain axis.

*Corresponding authors.
E-mail addresses: baoxiuqi@imm.ac.cn (Xiuqi Bao), danzhang@imm.ac.cn (Dan Zhang).

Peer review under the responsibility of Chinese Pharmaceutical Association and Institute of Materia Medica, Chinese Academy of Medical Sciences.

https://doi.org/10.1016/j.apsb.2025.02.029

1. Introduction

Parkinson's disease (PD) is a complex progressive and age related neurodegenerative disease[1]. Besides neuropathological damages in substantial nigra and motor dysfunction, a large number of PD patients suffer from gastrointestinal disorder, including intestinal barrier damage, decreased intestinal peristalsis and intestinal inflammation[2]. The aggregation of Lewy bodies was also found in intestine at the early stage of PD, suggesting that the gut might be an important affected organ of PD[3]. Enteric glia cells (EGCs) are unique peripheral nerve glial cells in the enteric nervous system, playing an important role in supporting the structure of gut and regulating intestinal functions, including intestinal inflammation[4], intestinal barrier function[5], and intestinal peristalsis[6] through complex interactions with intestinal neurons, immune cells, and epithelial cells. In PD patients, the expression of pro-inflammatory and gliosis markers involving glial fibrillary acidic protein (GFAP) and sex-determining region Y-box 10 (SOX-10) significantly increased in the colon mucous[7], indicating that EGCs might undergo reactive gliosis in PD. Moreover, our previous study has proved that inhibiting EGC gliosis could attenuate the pathological damages of PD, but how EGCs are regulated still needs to be clarified.

The gut microbiota, as a complex ecological community consisting of 100 trillion microorganisms[8], is capable of regulating EGCs by affecting their survival and regeneration. In the germ-free mice, the number of EGCs reduced, while the amount of EGCs increased after reconstitution of intestinal flora in the intestine[9], indicating that intestinal flora is necessary for the maintenance of EGC regeneration in the intestine. Moreover, intestinal flora affects the migration of EGCs, as less EGCs migrating to the lamina propria was observed in severe intestinal dysbiosis[10]. More importantly, gut microbiota dysbiosis could promote lipopolysaccharide (LPS) released or bacteria passing through the intestinal lumen and entering the inner layer of the intestinal wall, resulted in activating EGCs and triggering inflammation[9,11]. Gut microbiota communicates with the host in multiple ways, and microbial metabolites are believed to be critical intermediates to facilitate the interactions between gut microbiota and EGCs. A variety of microbial metabolites have been identified to be strongly related to PD pathogenesis, such as vitamin B12, indole derivatives, dopamine, tryptophan and secondary bile acid, etc.[12]; however, it still lacks of evidence showing which microbial metabolite is responsible for regulating EGC function in the progression of PD.

To address these issues, in the present study, we carried out a series of experiments to investigate the potential roles of intestinal flora on EGC gliosis in PD pathology and to identify the specific microbial metabolite which is capable of regulating EGC function. We found that gut microbiota dysbiosis occurred in PD mice, and was involved in EGC gliosis. We then identified the key differential metabolite 3-indolepropionic acid (IPA) that was able to inhibit EGC gliosis and inflammation. In addition, we proved the therapeutic effects of IPA on gut and brain in PD models, and clarified that IPA bound to pregnane X receptor (PXR) in EGCs, and then inhibited IL-13/IL-13Rα1 signaling and its downstream JAK1−STAT6 pathway, resulted in alleviated inflammation and pathological damages of PD. Our present study uncovered that IPA was the key microbial metabolite that inhibited EGC gliosis by suppressing PXR/IL-13Rα1/JAK1−STAT6 signaling pathways.

2. Material and methods

2.1. Animals and PD mouse model development

2.1.1. Animals

Male C57BL/6J mice weighing 22−25 g were obtained from Beijing HFK Bioscience Co., Ltd. (Beijing, China). Mice were kept under standard conditions (temperature 22 ± 2 °C and humidity 50%−60% on a 12 h light/dark cycle) with free to food and water ad libitum. They were allowed to acclimate to environment for three days before experimentation. All the experimental procedures were performed in accordance with the guidelines of the Beijing Municipal Ethics Committee for the care and use of laboratory animals, and were approved by the Animal Care & Welfare Committee, Institute of Materia Medica, CAMS&PUMC (Nos. 00007620, 00005402, and 00005071).

2.1.2. Development of rotenone-induced PD mouse model and treatments

Mice were orally administrated with freshly prepared rotenone (Sigma−Aldrich, MO, USA) solution (30 mg/kg, suspended in 0.5% CMC-Na) once a day for four weeks to induce PD pathological damage, and Control mice were treated with 0.5% CMC-Na. 3-Indolepropionic acid (IPA) (25, 50, 100 mg/kg suspended in 0.5% CMC-Na) was orally administrated once a day for 6 weeks. Fecal microbiota transplantation was treated to mice once a day for 2 weeks as described previously[13]. Control and rotenone-challenged mice were received vehicle administrations. GI functional evaluation and behavioral tests were performed at 6th week, respectively.

2.1.3. Development of 1-methyl-4-phenyl-1,2,3,6-tetrahydropyridine/probenecid (MPTP/p)-induced PD mouse model and treatments

Chronic PD mouse model was achieved by injection the combination of MPTP (Sigma−Aldrich) and probenecid (Sigma−Aldrich). Briefly, mice were intraperitoneally injected with probenecid (250 mg/kg, dissolved in DMSO) 30 min prior to subcutaneously injection of MPTP hydrochloride (25 mg/kg, dissolved in saline) to induce parkinsonian symptoms, while Control mice were injected with vehicles. These mice were received a total of 10 injections of MPTP in combination with probenecid. The 10 injections were given at an interval of 3.5 days for a 5-week schedule[14].

2.2. Motor behavior evaluations

2.2.1. Rotarod test

The rotarod test was performed as described previously[15]. Briefly, mice were positioned on the rod of rotarod apparatus (Ugo basile, Germany) and then tested on the revolving rod at the speed of 25 rpm for up to 120 s. The rotarod automatically recorded the

time that the animals first fell off the rod, which was designated as latency.

2.2.2. Grip strength test

The forepaws of the mice were allowed to grasp a horizontal rope which was 5 mm in diameter. Then the performance of each mouse on the rope was scored from 0 to 5 according to the criteria as followed: 0, falling off the rope in 10 s; 1, gripping the rope with only 1 forepaw; 2, gripping the rope with 2 forepaws; 3, gripping the rope with only 1 hind paw; 4, gripping the rope with 2 hind paws; 5, trying to escape to the end of the rope.

2.2.3. Beam walking test

The balance beam (Institute of Materia Medica, Chinese Academy of Medical Sciences) is a custom-built wooden bar (100 cm length × 6 cm width), placed 50 cm above the floor, with one end placed in a dark escape home cage. Testing was performed across three consecutive days. During the first two days, mice were habituated to the escape cage for 2 min, then placed at the starting point and trained to cross the balance beam to reach the escape cage three times. On the third day, mice were placed individually at the starting point and allowed to cross the balance beam. The number of foot-slips was recorded.

2.3. Fecal pellets output of PD mice

All the mice were forced to fast for 12 h, and then each mouse was free to eat for 2 h. Each mouse was arranged in a clean plastic cage and the gut motor function was evaluated by the number of fecal pellets collected at 5 min intervals for a 20 min period. Next, they stayed in the cages for another 1 h. Fecal pellets were collected and placed in sealed tubes. Subsequently, the numbers of fecal pellets were counted. The feces were weighed to get the wet weight, and dried at 65 °C for 24 h to obtain the dry weight. The water content was calculated according to the difference between the wet and dry fecal pellets weight[16].

2.4. Immunohistochemical analysis

In rotenone-induced PD mouse model experiment, mice were anesthetized with pentobarbital and perfused transcardially with saline and then with cold 4% paraformaldehyde in 0.1 mol/L phosphate buffer (pH 7.4) at the end of the 6th week. Brains were then removed and sectioned to 40 μm sections at the same position. Coronal sections through the substantia nigra were processed for TH immunohistochemistry as previously described[17]. Briefly, sections were incubated with rabbit polyclonal TH antibody (1:500, Abcam, CA, USA) and then incubated with the biotinylated secondary antibody and subsequently with avidin-peroxidase. Finally, the labeling was visualized with 0.05% 3,3′-diaminobenzidine (DAB). Images were captured by upright microscope (Nikon E600, Tokyo, Japan). The number of TH-positive cells were calculated by counting the number of TH-positive cells in the substantia nigra pars compacta by using ImageJ software.

2.5. Transmission electron microscopy

In the experiment of rotenone-induced PD mouse model, three mice were randomly selected for anesthesia and perfusion with 0.9 % saline at the end of 6th week. The brain and colon tissues were cut into pieces of 1 mm^3. Next, the fresh tissue sections were put into a fixing solution for transmission electron microscopy (TEM) (Servicebio, Wuhan, China) at 4 °C for 4 h and then fixed with 1% OsO_4 in 0.1 mol/L PBS for 2 h at room temperature, followed by dehydration with gradient alcohol. Subsequently, the sections were embedded by baking in an oven at 60 °C for 48 h and cut into ultrathin sections (60 nm) with ultramicrotome. Finally, the ultrastructure of tight junction of substantial nigra and colon were observed using a transmission electron microscope (HITACHI, HT7700, Japan).

2.6. Immunofluorescence staining for tissues

The colons and brains were removed and fixed in 4% paraformaldehyde for 24 h. And then the tissues were kept in 4% paraformaldehyde containing 30% sucrose. Colons and brains were embedded in paraffin and serially sliced at a 5 mm thickness. The immunofluorescence staining was performed following our previous research[17]. Briefly, the sections were deparaffinized and rehydrated. Next, they were immersed in sodium citrate solution (pH 6.0) for antigen retrieval. Subsequently, 3% bovine serum albumin (Servicebio, Wuhan, China) was added to block nonspecific binding and the slides were incubated overnight at 4 °C with the following primary antibodies: anti-GFAP (1:1000, Servicebio) and anti-SOX-10 (1:100, Abclonal) for colon staining, and anti-GFAP (1:600, Abcam, USA) and anti-Iba-1 (1:700, Abcam, USA) for brain staining. For colons staining, the objective tissues were covered with corresponding secondary antibodies: FITC labeled goat anti-mouse (1:400, Servicebio) and goat anti-rabbit IgGCY3 (1:300, Servicebio). For brain staining, the sections were incubated with horseradish peroxidase conjugated secondary antibody for 20 min (1:1000, Beijing Zhiyi Intellectual Property Agency). After washing, they were incubated with Opal 520 Fluorophore (1:100, Akoya Biosciences) and Opal 620 Fluorophore (1:100, Akoya Biosciences) for 10 min. Both nuclei were stained using DAPI solution. The images were observed with fluorescent microscopy (Nikon Eclipse C1, Tokyo, Japan) and the number of positively stained cells was calculated using Image J 6.0 software. All evaluations were done by a researcher blinded to the experiment.

2.7. 16S rRNA gene sequencing

Feces were collected and frozen instantly and stored at −80 °C prior to analyzed. Total genome DNA from stool sample was extracted using CTAB/SDS method. DNA concentration and purity was monitored on 1% agarose gels, and was diluted to 1 ng/μL using sterile water. 16S rRNA/18SrRNA/ITS genes of distinct regions (16S V4/16S V3/16S V3−V4/16S V4−V5, 18S V4/18S V9, ITS1/ITS2, Arc V4) were amplified using specific primer (*e.g.*,16S V4: 515F-806R, 18S V4: 528F-706R, 18S V9: 1380F-1510R) with the barcode. All PCR reactions were carried out with 15 μL of Phusion® High-Fidelity PCR Master Mix (New England Biolabs), 0.2 μmol/L of forward and re*verse* primers, and about 10 ng template DNA. Thermal cycling consisted of initial denaturation at 98 °C for 1 min, followed by 30 cycles of denaturation at 98 °C for 10 s, annealing at 50 °C for 30 s, elongation at 72 °C for 30 s, and finally 72 °C for 5 min. Mix the same volume of 1 × loading buffer (contained SYBR green) with the PCR products and subjected to electrophoresis on 2% agarose gel for detection. PCR products was mixed in equinity ratios. Then, the mixture of PCR products was purified with Qiagen Gel Extraction Kit (Qiagen, Germany). Sequencing libraries were generated

usingTruSeq® DNA PCR-Free Sample Preparation Kit (Illumina, USA) following manufacturer's recommendations and index codes were added. The library quality was assessed on the Qubit@ 2.0 Fluorometer (Thermo Scientific) and Agilent Bioanalyzer 2100 system. At last, the library was sequenced on an Illumina NovaSeq platform and 250 bp paired-end reads were generated.

2.8. T3 UPLC conditions and ESI-QTRAP-MS/MS for non-targeted metabolomics

The feces, blood and urine were collected, and were processed with grinding and centrifugation. Then, a 200 μL aliquots of supernatant obtained from the pretreated samples were transferred into vials and undergoing the LC−MS analysis. The sample extracts were analyzed using an LC−ESI-MS/MS system (UPLC, ExionLC AD, https://sciex.com.cn/; MS, QTRAP® System, https://sciex.com/). The analytical conditions were as follows, UPLC: column, Waters ACQUITY UPLC HSS T3 C18 (1.8 μm, 2.1 mm × 100 mm); column temperature, 40 °C; flow rate, 0.4 mL/min; injection volume, 2 μL; solvent system, water (0.1% formic acid): acetonitrile (0.1% formic acid); gradient program, 95:5 *v/v* at 0 min, 10:90 *v/v* at 11.0 min, 10:90 *v/v* at 12.0 min, 95:5 *v/v* at 12.1 min, 95:5 *v/v* at 14.0 min. LIT and triple quadrupole (QQQ) scans were acquired on a triple quadrupole-linear ion trap mass spectrometer (QTRAP), QTRAP® LC−MS/MS System, equipped with an ESI Turbo Ion−Spray interface, operating in positive and negative ion mode and controlled by Analyst 1.6.3 software (Sciex). The ESI source operation parameters were as follows: source temperature 500 °C; ion spray voltage (IS) 5500 V (positive), −4500 V (negative); ion source gas I (GSI), gas II (GSII) and curtain gas (CUR) were set at 55, 60, and 25 psi, respectively; the collision gas (CAD) was high. Instrument tuning and mass calibration were performed with 10 and 100 μmol/L polypropylene glycol solutions in QQQ and LIT modes, respectively. A specific set of MRM transitions was monitored for each period according to the metabolites eluted within this period.

2.9. Bioinformatics analysis

Paired-end reads were assigned to samples based on their unique barcode and truncated by cutting off the barcode and primer sequence, and merged using FLASH (V1.2.7, http://ccb.jhu.edu/software/FLASH/), a very fast and accurate analysis tool, which was designed to merge paired-end reads when at least some of the reads overlap the read generated from the opposite end of the same DNA fragment, and the splicing sequences were called raw tags. Quality filtering on the raw tags were performed under specific filtering conditions to obtain the high-quality clean tags according to the QIIME (V1.9.1, http://qiime.org/scripts/split_libraries_fastq.html) quality control process. The tags were compared with the reference database (Silva database, https://www.arbsilva.de/) using UCHIME algorithm (UCHIME Algorithm, http://www.drive5.com/usearch/manual/uchime_algo.html) to detect chimera sequences, and then the chimera sequences were removed and the Effective Tags were finally obtained.

The mass spectrum data was processed using Analyst 1.6.3 software. All data analysis was based on the self-built MWDB database (Metware Biotechnology Co., Ltd. Wuhan, China). The principal component analysis (PCA) and latent structures-discriminant analysis (OPLS-DA) were generated using R package MetaboAnalystR (v1.0.1). Significantly regulated metabolites between groups were determined by Variable Importance in Projection (VIP) value and Fold Change (FC) value, where VIP≥1 and Fold Change≥1.2 or Fold Change≤0.83 FC were considered to be significant in the experimental groups (Control and MPTP/p). The differential metabolites were annotated by KEGG compound database (http://www.kegg.jp/kegg/compound/) and then mapped to the KEGG pathway database (http://www.kegg.jp/kegg/pathway.html).

2.10. Cell culture and treatments

EGCs were purchased from Hunan FengHui biotechnology Co., Ltd. The cells were grown in Dulbecco's modified Eagle's medium (DMEM, Solarbio, Beijing, China), supplemented with 10% fetal bovine serum (Sijiqing, Hangzhou, China), 100 U/mL penicillin and 100 μg/mL streptomycin, and were kept at 37 °C in a humidified 5% CO_2 air incubator. The cells were incubated with IPA at the concentration of 0.1 μmol/L, and challenged with 600 nmol/L rotenone for 72 h. To inhibit Aryl hydrocarbon Receptor (AhR), the EGCs cells were incubated with its inhibitor, PDM2 (TargetMol, Shanghai, China) at concentration of 100 nmol/L. To investigate the inhibition of PXR and IL-13Rα1, EGCs were transfected with the PXR siRNA and IL-13Rα1 siRNA, respectively (Sangon Biotech, Shanghai, China) or negative control siRNA (Sangon Biotech, Shanghai, China) using Lipofectamine RNAiMAX Transfection Reagent (Sangon Biotech, Shanghai, China) and then seeded in 6 cm plate. 24 h after transfection, cells were incubated with IPA at the concentration of 0.1 μmol/L, and then challenged with 600 nmol/L rotenone for another 72 h.

2.11. Immunofluorescence staining for cells

For immunofluorescence staining, the cells were plated on 24-well culture plates at a density of 1.5×10^4 cells/well. The cell culture media was removed and the cells were fixed in 4% paraformaldehyde for 30 min at room temperature and washed three times with PBS. The cells were permeabilized in 0.1% TritonX-100 (Sigma−Aldrich) for 10 min and blocked in 3% goat serum for 1h at room temperature. After an overnight incubation with the anti-GFAP antibody (1:500, Abcam, CA, USA) at 4 °C, the cells were washed three times with 1 × PBS and then incubated with secondary antibody (1:200 dilution, Abcam) for 1 h at room temperature. Afterwards, the cells were washed three times with 1 × PBS and stained with 4,6-diamidino-2-phenylindole (DAPI, Gentihold, Beijing, China) for 5 min at room temperature. Coverslips were examined and photographed under a confocal microscope (Leica, Weztlar, Germany) with a Leica TCS SP8 system.

2.12. Quantitative polymerase chain reaction assay (qPCR)

The total RNA was isolated from the EGCs using the TransZol Up Plus RNA kit (TransGen Biotech Co., Beijing, China) according to the manufacturer's instructions. Then the amount of RNA was reversely transcribed to cDNA using TransScript One-Step gDNA Removal and cDNA Syn-thesis SuperMix (TransGen Biotech Co.). qPCR assay of different genes was detected by TransStart Tip Green qPCR SuperMix (+DyeI/−DyeII) (TransGen Biotech Co.), and the mRNA was amplified for qPCR with the following primers shown in Supporting Information Table S1. Amplification was run in the 7900HT Fast Real-Time PCR system (Applied Biosystems, Foster City, CA, USA) at 94 °C for 30 s followed by

40 cycles of 94 °C for 5 s, 59 °C for 15 s, and 72 °C for 10 s, then 95 °C for 15 s as a final elongation step. The relative quantification of mRNA expression was calculated by $2^{-\Delta\Delta Ct}$ algorithms.

2.13. Genome-wide RNA sequencing and analysis

A total amount of l μg RNA per sample was used as input material for the RNA sample preparations. Sequencing libraries were generated using NEBNextRUltraTMRNA Library Prep Kit for lluminaR (NEB, USA) following manufacturer's recommendations and index codes were added to attribute sequences to each sample. Briefly, mRNA was purified from total RNA using poly-T oligo attached magnetic beads. Fragmentation was carried out using divalent cations under elevated tecmperature in NEBNext First Strand Synthesis Reaction Buffer (5 ×). First strand cDNA was synthesized using random hexamer primer and M-MuLVReverse Transcriptase (RNase H−). Second strand cDNA synthesis was subsequently performed using DNA Polymerase I and RNase Remaining overhangs were converted into blunt ends *via* exonuclease/polymerase activities. After adenylation of 3′ ends of DNA fragments, NEBNext Adaptor with hairpin loop structure were ligated to prepare for hybridization. In order to select cDNA fragments of preferentially 250−300 bp in length, the library ragments were purified with AMPure XP system (Beckman Coulter, Beverly, USA). Then 3 μL USER Enzyme (NEB, USA) was used with size-selected, adaptor-ligated cDNA at 37 °C for 15 min followed by 5 min at 95 °C before PCR. Then PCR was performed with Phusion High-Fidelity DNA polymerase, Universal PCR primers and Index (X) Primer. At last, PCR products were purified (AMPure XP system) and library quality was assessed on the Agilent Bioanalyzer 2100 system. After cluster generation, the library preparations were sequenced on an illumina platform and 150 bp paired-end reads were generated.

2.14. Western blot

Cells, midbrain, and colon were collected, and they were lysed in radioimmunoprecipitation assay (RIPA) lysate buffer (Sangon Biotech, Shanghai, China) with protease phosphatase inhibitor (Solarbio, Beijing, China) and protease inhibitor (Targetmol, Shanghai, China). Nuclear proteins were obtained using the nuclear-cytosol extraction kit (APPLYGEN, Beijing, China). The total protein concentrations were determined by bicinchoninic acid (BCA) kit (Yeasen, Shanghai, China) to ensure equal sample loading. Following our previous descriptions[18], proteins were separated by SDS−polyacrylamide gels (10%) and transferred into a 0.45 μm polyvinylidene fluoride membrane (Millipore, USA), which were then blocked with 5% skim milk-TBST (20 mmol/L of Tris−HCl, pH 7.5, and 500 mmol/L of NaCl, 0.1% Tween 20) for 2 h. The membranes were probed with the following antibodies: Aryl hydrocarbon Receptor (AhR) (1:1000, Thermo Fisher Scientific, MA USA); Interleukin-13 receptor subunit alpha-1 (IL-13Rα1) (1:500, Santa Cruz, CA, USA); β-actin (1:10,000), GAPDH (1:10,000), Pregnane X receptor (PXR) (1:1000), occludin (1:1000), sex-determining region Y-box 10 (SOX-10) (1:1000), Janus kinase1 (JAK1) (1:1000), Signal transducer and activator of transcription 6 (STAT6) (1:1000) and claudin-1 (1:1000, Abclonal, Wuhan, China); tyrosine hydroxylase (TH) (1:1000, Cell Signaling Technology, Boston, USA); glial fibrillary acidic protein (GFAP) (1:1000), inducible nitric oxide synthase (iNOS) (1:1000), cyclooxygenase 2 (COX-2) (1:1000), phosphorylated-Janus kinase1 (*p*-JAK1) (1:1000), phosphorylated-signal transducer and activator of transcription 6 (p-STAT6) (1:1000, Abcam, CA, USA) and Zonula occludens protein 1 (ZO-1) (1:1000, Proteintech, Wuhan, China), overnight at 4 °C; and then these were incubated with horseradish peroxidase (HRP) goat anti-rabbit IgG (1:2000, Abclonal, Wuhan, China) for 2 h at room temperature. The blots were visualized by incubating the membranes with ECL Plus reagents (Yeasen, Shanghai, China) and the images were recorded by LAS-4000 chemiluminescence system (Fujifilm, Tokyo, Japan). The blot densities were assessed by Gel-pro analyzer 4.0 (Media Cybernetics, MD, USA).

2.15. Statistical analysis

Statistical analysis was conducted using Graphpad6.02 software. Data are presented as the mean ± standard error of mean (SEM). Two-tailed unpaired Student's *t*-test was used when comparing two groups, and one-way ANOVA with Tukey's correction was used to compare the means of three or more groups, and correlation analysis of gut microbiome and gut metabolites were performed using nonparametric Spearman's test or Pearson's test. $P < 0.05$ was considered statistically significant.

3. Results

3.1. IPA was the main differential intestinal microbial metabolite in PD mice contributing to the regulation of EGCs

Recent data suggested that EGCs may play a major role in PD-related gastrointestinal disturbances, as well as in the development and progression of the central disease[19]. Consistent with these studies, our previous study has proved that inhibition of EGCs gliosis could alleviate gut and dopaminergic neuronal dysfunction in PD mice. In the present study, we further investigated whether and how EGCs were regulated by gut microbiota in the process of PD pathology. Our study showed that gut microbiota dysbiosis occurred in rotenone-induced PD mice (Fig. 1A and B), along with abnormally activated EGCs, as detected by upregulated GFAP and SOX-10 in rotenone-induced PD models (Fig. 1C and D). After transplantation fecal microbiota of control mice to PD mice, EGC activation was significantly inhibited (Fig. 1C and D), indicating that EGC function could be regulated by gut microbiota. We then continued to investigate the significant microbial metabolite that was probably responsible for regulating the function of EGCs. Our data showed that there were 3 genera of bacteria were identified as differential flora in the feces of MPTP/p-induced PD mice by 16S rRNA analysis, including increased abundance of *Lachnospiraceae_UCG-006*, *Gemella* and decreased abundance of *Peptococcus* (Fig. 1E). By metabolomic study, 48 differential metabolites overlapped in urine, plasma, and feces were identified (Fig. 1F). Through analyzing the 48 differential metabolites, there were 29 significant differential metabolites probably related to PD. Among them, we found that only 2-ethyl-2-hydroxybutyric acid, 3-epideoxycholic acid, IPA, acrylamide and D-mannose were highly correlated to more than one differential gut microbiota, while others either had no correlated differential gut microbiota or only related to one differential gut microbiota (Fig. 1G). Further correlation analysis between pathological indexes of PD (*e.g.*, the time staying on the rotarod and performance score of climbing) and these 5 differential metabolites revealed that IPA was the most relevant metabolite to these indexes with the highest correlation coefficient (Fig. 1H). Apart from differential microbiota that related to IPA in MPTP/p-

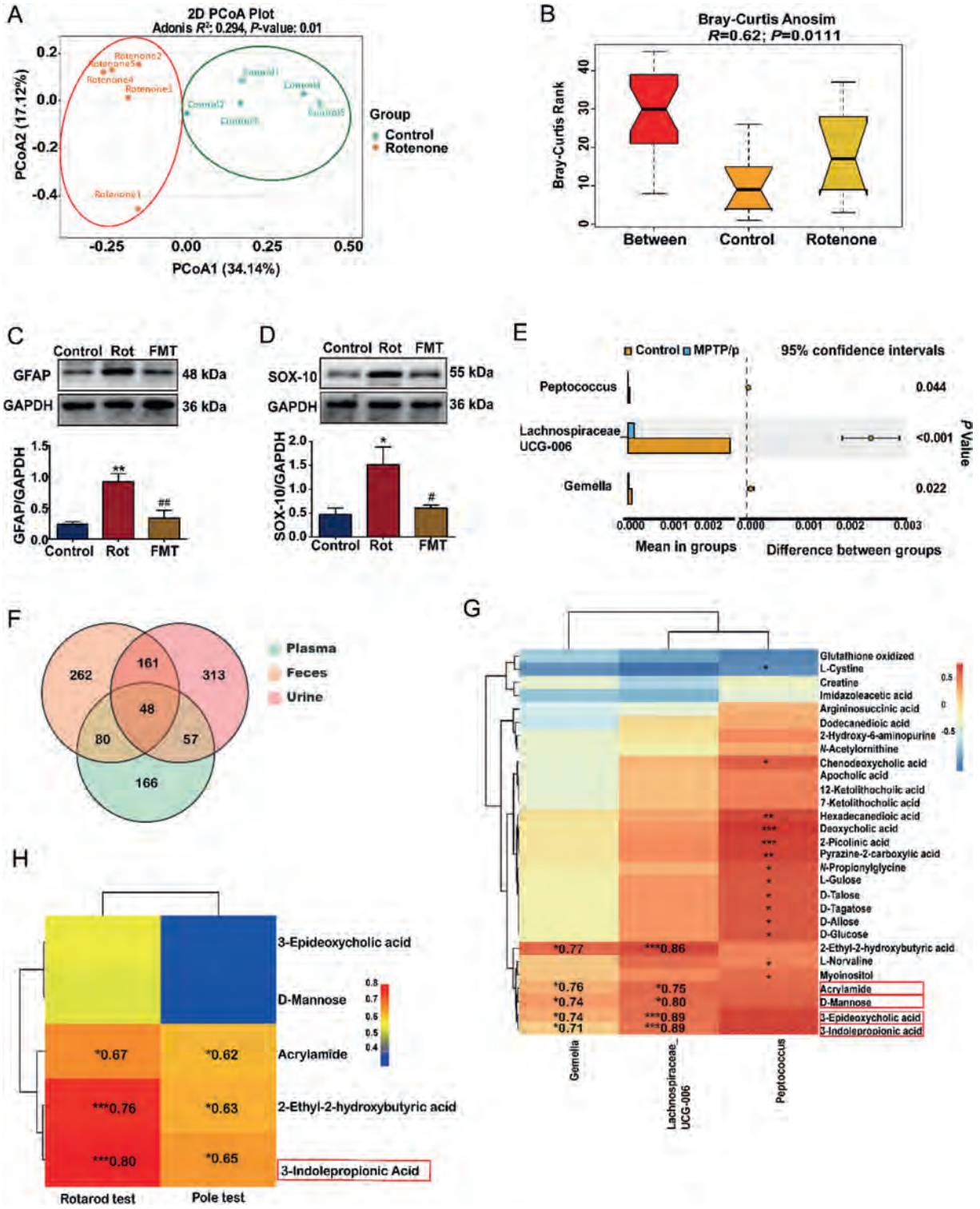

Figure 1 IPA was the main differential intestinal microbial metabolite in PD mice contributing to the regulation of EGCs. Mice were treated with rotenone for four weeks, and then the fecal pellets were collected from five mice. (A) PCoA weighted UniFrac Adonis analysis and (B) ANOISM analysis of 16S rRNA from five mice. (C) Western blot analysis of GFAP and (D) SOX-10 expression after FMT from 4 to 6 mice. Data are presented as mean ± SEM. $^{*}P < 0.05$, $^{**}P < 0.01$ *versus* Control mice; $^{\#}P < 0.05$, $^{\#\#}P < 0.01$ *versus* PD mice. The mice were treated with MPTP/p for five weeks, and then the fecal pellets were collected for 16S rRNA analysis. Feces, plasma and urine were collected and subjected to untargeted metabolomic analysis. (E) Analysis at the genus level of gut microbiota between Control mice and MPTP/p-induced PD mice from four mice. (F) Overlapped differential metabolites shown in the Venn plot of metabolomics analysis from six mice. (G) Ellipse heatmap of spearman correlation analysis between differential metabolites and differential gut microbiota. Spearman analysis. (H) Heatmap of Pearson correlation between pathological indexes and differential metabolites. Pearson analysis, $^{*}P < 0.05$, $^{**}P < 0.01$, $^{***}P < 0.001$.

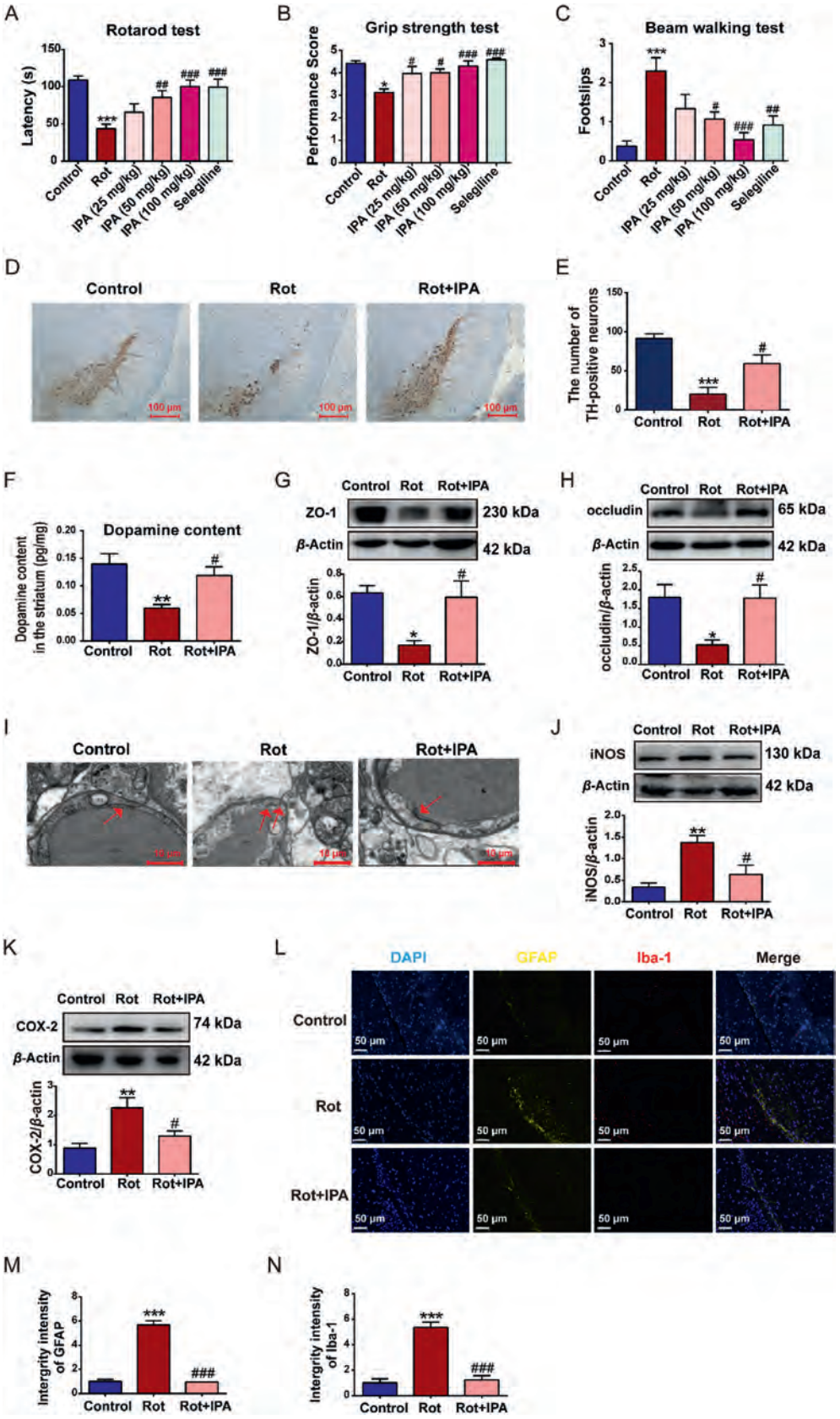

Figure 2 IPA alleviated neuropathological damage and improved motor coordination in PD mice. The rotenone-induced PD mice were treated with IPA (25, 50, and 100 mg/kg) for 6 weeks, and then 12−20 mice in each group were subjected to motor function tests. (A) Rotarod tests. (B) Grip strength tests. (C) Footslips in the beam walking tests. The rotenone-induced PD mice were treated with IPA (50 mg/kg) for 6 weeks, and then the midbrain and striatum were collected after motor behavior tests. (D) Immunohistochemistry of TH staining in substantia nigra. Representative sections of the substantia nigra from three mice were shown. Scale bar: 100 μm. (E) Numbers of TH positive cells were counted in each group. (F)

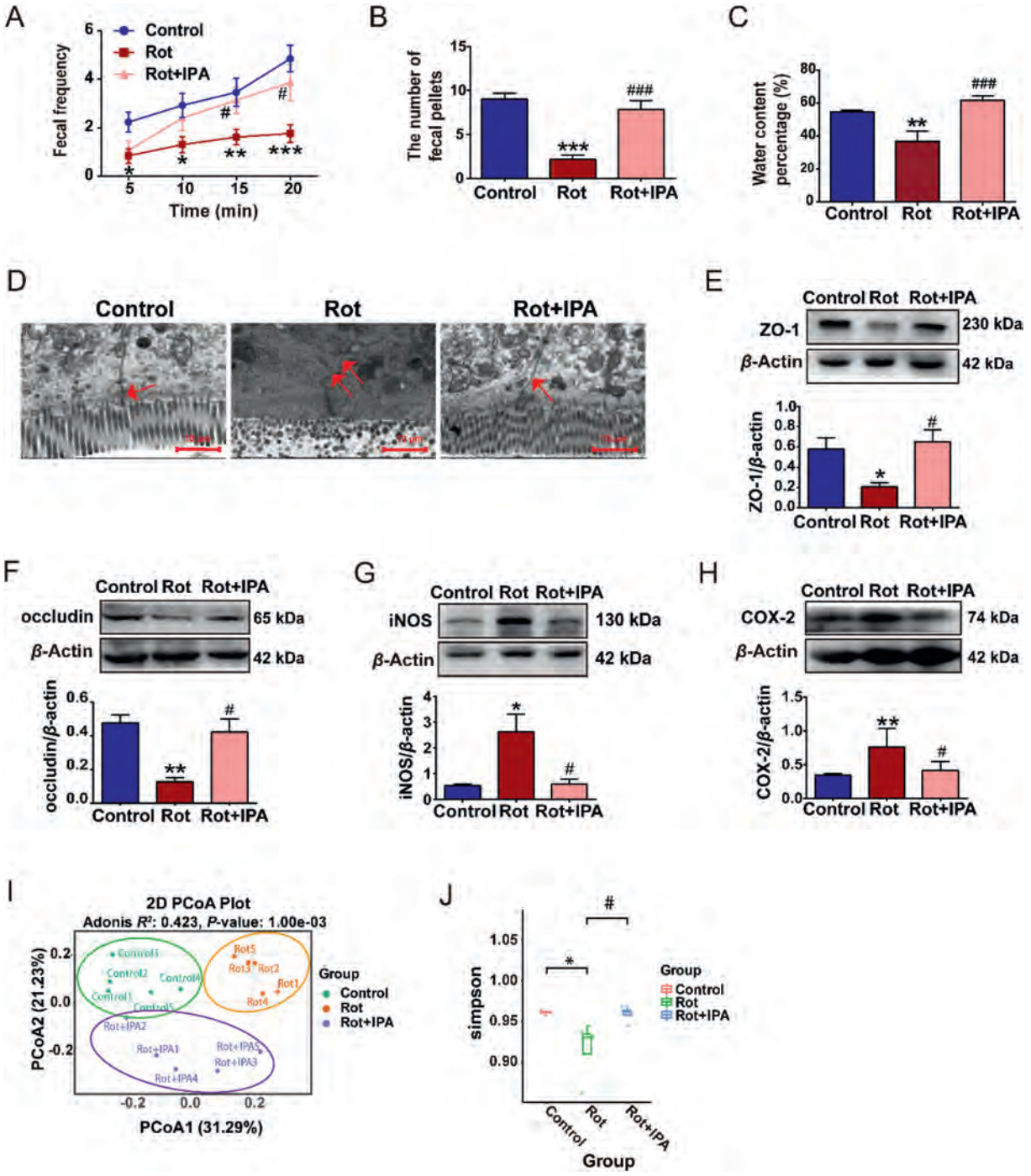

Figure 3 IPA suppressed gut inflammation and improved intestinal function in PD mouse model. Rotenone-induced PD mice were treated with IPA (50 mg/kg) for 6 weeks, and then the colon and feces were collected. (A) Fecal frequency, (B) Fecal pellet output, and (C) Water content percentage from 13 to 15 mice. (D) Representative electron micrographs showing the tight junction structure of gut barrier from three mice (red arrow). Scale bar: 10 μm. Western blot analysis of (E) ZO-1 and (F) occludin expression. Western blot analysis of (G) iNOS and (H) COX-2 treated with IPA. Represent images of Western blot were from 4 to 6 independent experiments. (I) PCoA bray curtis analysis after IPA treatment. (J) The Simpson analysis after IPA treatment. Data are presented as mean ± SEM. $^{*}P < 0.05$, $^{**}P < 0.01$, $^{***}P < 0.001$ *versus* Control mice; $^{\#}P < 0.05$, $^{\#\#}P < 0.01$, $^{\#\#\#}P < 0.001$ *versus* PD mice.

Dopamine content in the striatum from 4 to 6 mice. (G) Western blot analysis of ZO-1 expression. (H) Western blot analysis of occludin expression. Represent images of Western blot were from 4 to 6 independent experiments. (I) Representative electron micrographs showed the tight junction structure in substantial nigra from three mice (red arrow). Scale bar: 10 μm. (J) Western blot analysis of iNOS expression. (K) Western blot analysis of the COX-2 expression. (L) GFAP (yellow), Iba-1 (red), and DAPI (blue) immunoreactivity in substantial nigra, and relative immunolabeling quantifications of (M) GFAP, (N) Iba-1 from three mice. Scale bar: 50 μm. Data are presented as mean ± SEM. $^{*}P < 0.05$, $^{**}P < 0.01$, $^{***}P < 0.001$ *versus* Control mice; $^{\#}P < 0.05$, $^{\#\#}P < 0.01$, $^{\#\#\#}P < 0.001$ *versus* Rotenone-challenged mice.

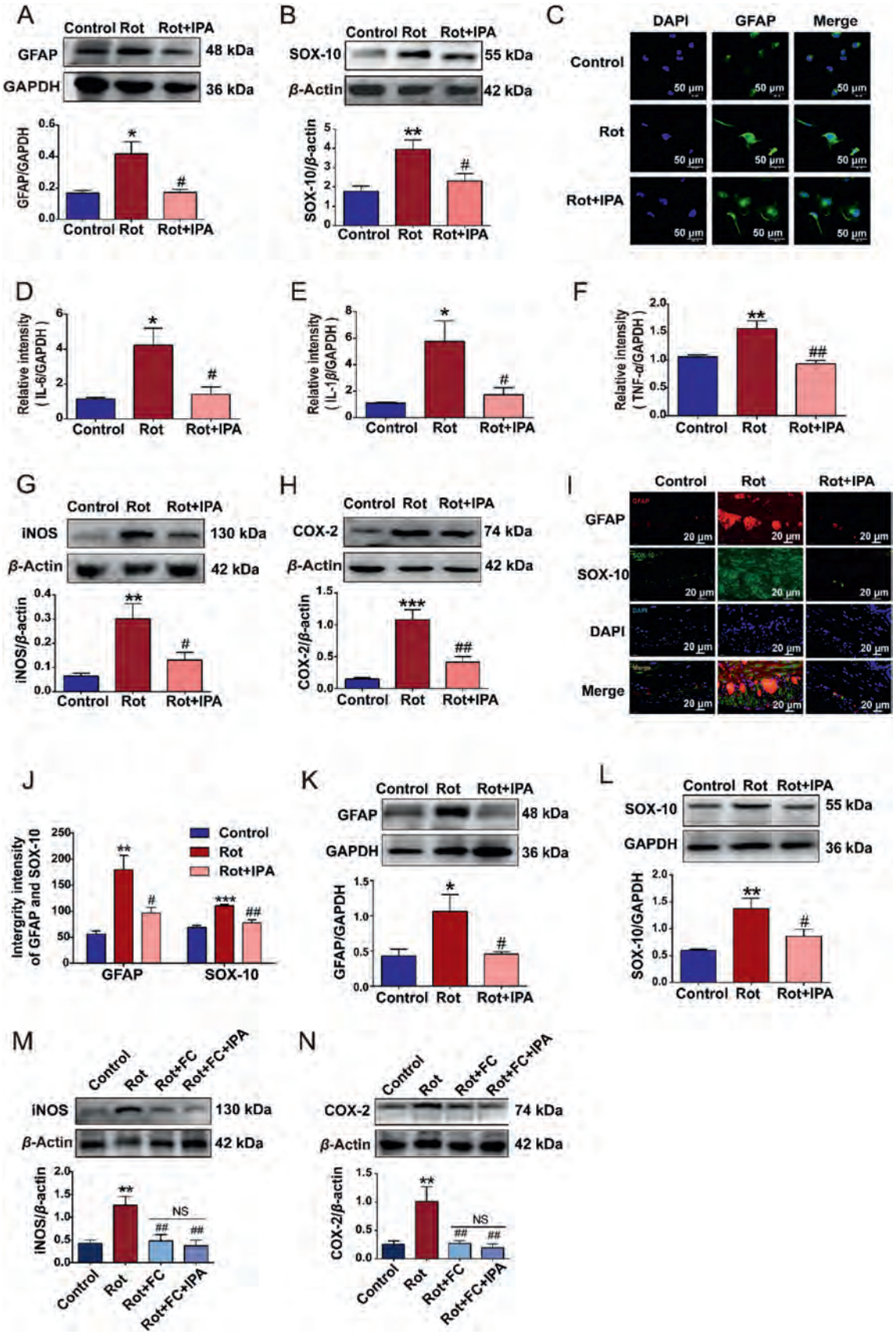

Figure 4 IPA inhibited EGC gliosis in rotenone-induced *in vitro* and *in vivo* PD models. EGCs were stimulated with rotenone and treated with IPA for 72 h. (A) Western blot analysis of the GFAP. (B) Western blot analysis of the SOX-10. (C) Confocal microscopy detection of GFAP. Represent images of immunofluorescence were from four independent experiments. Scale bar:50 μm. (D) the mRNA level of IL-6, (E) the mRNA

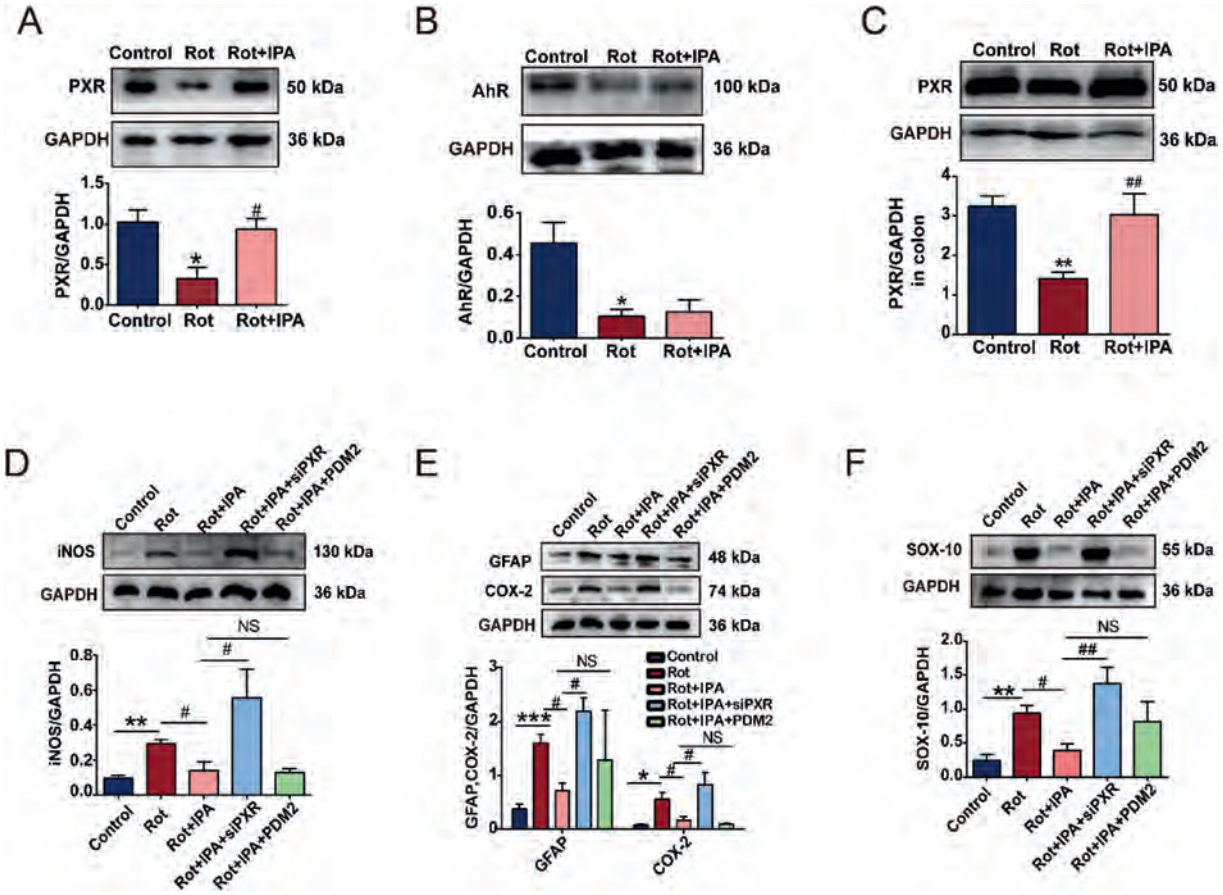

Figure 5 IPA targeted PXR to decrease the EGC reactive gliosis and inflammation. EGCs or mice were challenged with rotenone, and then treated with IPA. (A) Western blot analysis of PXR in EGCs. (B) Western blot analysis of the AhR in EGCs. Rotenone-induced PD mice were treated with IPA (50 mg/kg) for 6 weeks, and then the colon was collected. (C) Western blot analysis of the PXR in the colon of PD mice. EGCs were either transfected with PXR siRNA or treated with AhR antagonist, and then stimulated with rotenone in the presence or absence of IPA. (D) Western blot analysis of iNOS after knockdown PXR. (E) Western blot analysis of GFAP and COX-2 after knockdown PXR. (F) Western blot analysis of SOX-10 after knockdown PXR. Represent images of Western blot were from 4 to 6 independent experiments. Data are presented as mean ± SEM. $^{*}P < 0.05$, $^{**}P < 0.01$, $^{***}P < 0.001$ *versus* Control cells (mice); $^{\#}P < 0.05$, $^{\#\#}P < 0.01$, $^{\#\#\#}P < 0.001$ *versus* Rotenone-challenged cells (mice).

induced PD mice, we also found differential microbiota that were reported to be strongly correlated to IPA production in rotenone-induced PD mice, including decreased abundance of unidentified *Ruminococcaceae* and *Turicibacter*[20-22] (Supporting Information Fig. S1). The above results demonstrated that the reduced production of microbial metabolite IPA did present in PD mouse models, and gut microbiota may regulate EGC function through its metabolite IPA.

3.2. IPA alleviated neuropathological damage and improved motor coordination in PD mice

We then further investigated whether IPA could attenuate neuroinflammation and exert beneficial effects on dopaminergic neurons and motor coordination in PD mouse model. Our data showed that IPA at 25, 50 and 100 mg/kg dose-dependently improved motor coordination in rotenone-induced PD mice, as indicated by increased time of mice staying on the rod in rotarod test (Fig. 2A), improved performance behaviors in grip strength test (Fig. 2B) and decreased footslips in beam walking test (Fig. 2C). Among the three doses, 50 and 100 mg/kg showed statistically differences (Fig. 2A–C), so we selected 50 mg/kg IPA for further investigations. We found that IPA treatment could alleviate neuropathological damage in substantia nigra by decreasing α-synuclein expression (Supporting Information Fig. S2A and S2B), increasing the number of TH positive neurons (Fig. 2D and E) and TH expression (Fig. S2C), as well as increasing dopamine content in the striatum of PD mice (Fig. 2F). Moreover, IPA treatment

level of IL-1β and (F) the mRNA level of TNF-α from three mice in each group. (G) Western blot analysis of the iNOS. (H) Western blot analysis of the COX-2. Represent images of Western blot were from 4 to 6 independent experiments. Rotenone-induced PD mice were treated with IPA (50 mg/kg) or IPA + FC (20 μmol/kg) for 6 weeks, and then the colon was collected. (I) GFAP (red), SOX-10 (green), and DAPI (blue) immunoreactivity and (J) relative immunolabeling quantification from three mice. Scale bar: 20 μm. (K) Western blot analysis of the GFAP in colon. (L) Western blot analysis of the SOX-10 in colon. Western blot analysis of (M) iNOS and (N) COX-2 treated with IPA in the presence or absence of FC treatment. Represent images of Western blot were from 4 to 6 independent experiments. Data are presented as mean ± SEM. $^{*}P < 0.05$, $^{**}P < 0.01$, $^{***}P < 0.001$ *versus* Control cells (mice); $^{\#}P < 0.05$, $^{\#\#}P < 0.01$, $^{\#\#\#}P < 0.001$ *versus* Rotenone-challenged cells (mice).

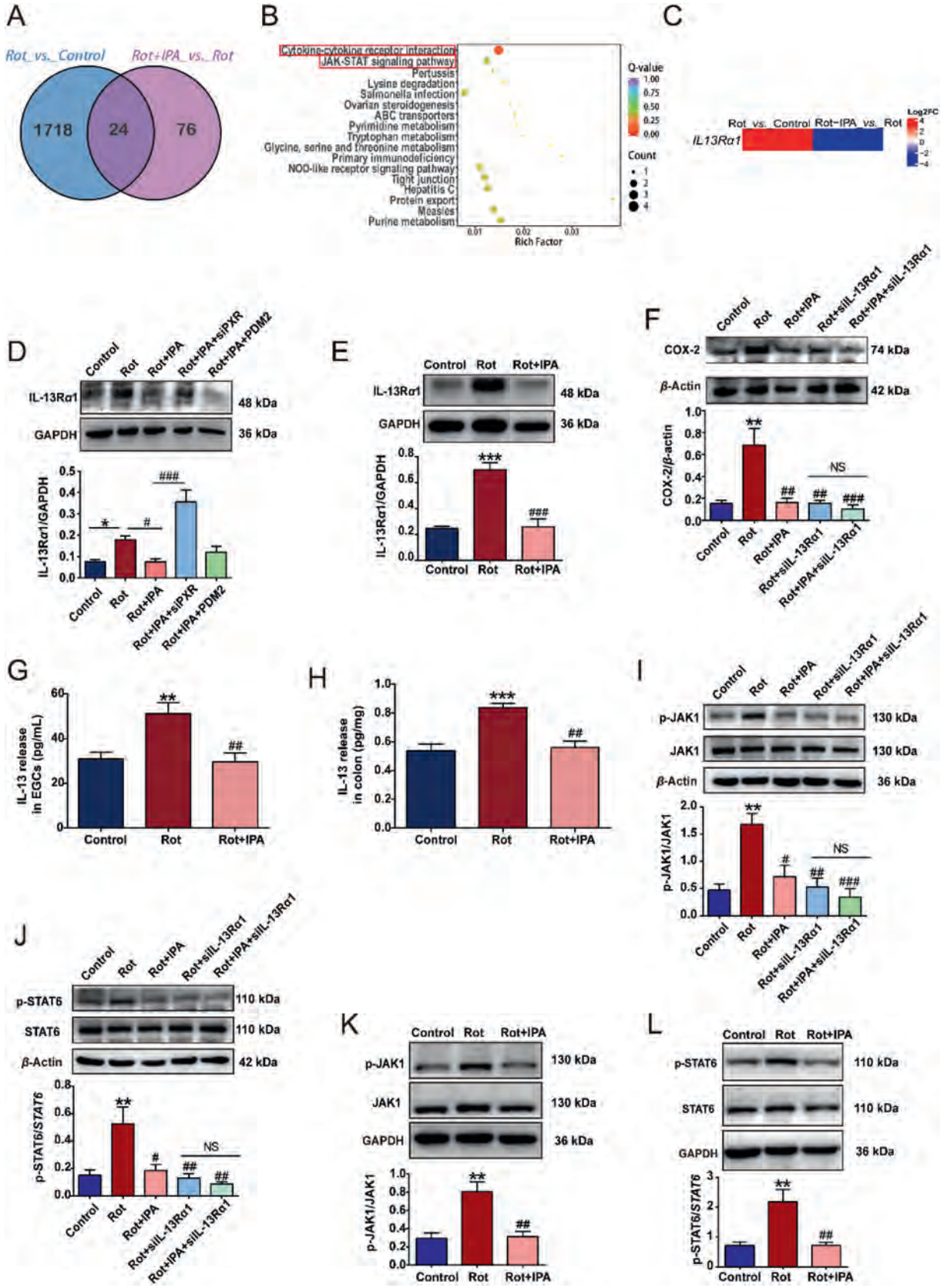

Figure 6 IPA decreased the EGC reactive gliosis and inflammation though suppressing IL-13Rα1 signaling pathways. EGCs were either transfected with PXR siRNA or treated with AhR antagonist or IL-13Rα1 siRNA, and then stimulated with rotenone in the presence or absence of IPA. (A) Venn-diagram of differential expression of the genes following treatment with IPA in EGCs. (B) The bubble plot of KEGG pathway enrichment. (C) Heatmap of differentially expressed genes regulated by IPA treatment. (D) Western blot analysis of IL-13Rα1 in EGCs. (E)

improved brain barrier function by increasing the expression of ZO-1 and occludin (Fig. 2G and H), improving ultrastructure of brain barrier in substantial nigra in PD mice (Fig. 2I). In addition, the data showed that the expression of inflammation-related proteins, iNOS and COX-2 in the midbrain (Fig. 2J and K) and the expression of GFAP and Iba-1 in substantial nigra, markers of astrocytes and microglia, respectively (Fig. 2L−N), were markedly reduced after PD mice were treated with IPA. Furthermore, we found that IPA treatment could significantly decreased the level of LPS and LBP in the midbrain (Fig. S2D and S2E). These results demonstrated that the intestinal flora metabolite IPA had neuroprotective activity on PD mice.

3.3. IPA suppressed gut inflammation and improved intestinal function in PD mouse model

Furthermore, the therapeutic effects of IPA on rotenone-induced gut dysfunction were investigated. IPA treatment markedly improved the gut function by increasing the fecal frequency (Fig. 3A), fecal output in 1 h (Fig. 3B), and water content percentage (Fig. 3C). Moreover, the damaged intestinal barrier was also attenuated by IPA treatment, indicated as restoration of tight junctions (Fig. 3D), as well as increased expression of ZO-1 and occludin (Fig. 3E and F). The therapeutic effects of IPA on suppressing gut inflammation in PD mice were further investigated. Our data showed that IPA treatment significantly decreased the expression of iNOS (Fig. 3G) and COX-2 (Fig. 3H), as well as LPS and LBP concentrations (Supporting Information Fig. S3A and S3B) in the colon, suggesting that IPA was able to suppress gut inflammation. We also found that IPA could suppress systemic inflammation by decreasing TNF-α, IL-1β, LPS and LBP in the circulating blood (Fig. S3C−S3F). It was worth noting that IPA treatment could alleviate the microbiota dysbiosis by improving the richness and abundance of intestinal flora in rotenone-induced PD mice (Fig. 3I and J), further supporting that IPA was closely correlated with intestinal flora. Taken together, these results demonstrated that IPA could alleviate intestinal pathological damage and improve gut function through rescuing inflammation in PD mice.

3.4. IPA inhibited EGC gliosis in rotenone-induced in vitro and in vivo PD models

We carried out experiments to further explore whether IPA improved gut and motor functions through inhibiting EGC gliosis and its mediated inflammation. In rotenone-challenged EGCs, IPA at 0.1 μmol/L significantly inhibited EGC activation by reducing the expression of GFAP and SOX-10 (Fig. 4A−C). Moreover, IPA markedly decreased EGCs mediated inflammation stimulated by rotenone, indicated as reduced mRNA expression of IL-6, IL-1β and TNF-α (Fig. 4D−F), as well as decreased protein expression of iNOS and COX-2 (Fig. 4G and H). Our data also showed that IPA treatment significantly decreased EGC activation and inflammation *in vivo* by reducing the expression of GFAP, SOX-10 detected by Immunofluorescence (Fig. 4I and J) and Western blot (Fig. 4K and L) in the colon of PD mice. More importantly, we revealed that IPA mainly targeted EGCs to exert the therapeutic effects in the colon of PD mice, as additional IPA treatment after suppressing EGC gliosis by FC could not further decrease the expression of iNOS and COX-2 (Fig. 4M and N). The above results strongly illustrated that IPA protected gut function through inhibiting EGC gliosis and inflammation, further exerting therapeutic effects on PD *via* gut−brain axis.

3.5. IPA targeted PXR to decrease EGC reactive gliosis and inflammation

It is reported that AHR and PXR were the main endogenous receptors of IPA[23,24], mediating the anti-inflammatory effect of IPA. In the present study, we aimed to elucidate which receptor was responsible for the inhibition of EGCs by IPA. Our data showed that the expression of PXR was increased after IPA treatment in both rotenone-challenged EGCs (Fig. 5A) and the colon of PD mice (Fig. 5C), while AhR expression was not changed (Fig. 5B). Further study by knocking down PXR in EGCs showed that the expression of reactive gliosis markers, GFAP and SOX-10, as well as inflammatory proteins, iNOS and COX-2, were remarkably elevated in the presence of IPA, while the expressions of these four proteins were not significantly changed when AhR was inhibited by PDM2 (Fig. 5D−F). These data suggested that IPA might mainly target PXR in EGCs to suppress inflammation.

3.6. IPA mainly decreased the EGC reactive gliosis and inflammation in gut via PXR− IL-13Rα1−JAK1−STAT6 pathway

We then conducted genome-wide transcriptomic analysis to uncover the molecular mechanisms underlying the therapeutic effects of IPA on PD. The data showed that 24 differential genes were markedly changed when the cells were treated with IPA compared to rotenone stimulated alone (Fig. 6A). The KEGG enrichment analysis of these 24 differential genes showed that cytokine−cytokine receptor interaction and JAK−STAT signaling pathways were with higher enrichment scores among the top 20 signaling pathways (Fig. 6B). Analysis of these 24 differential genes showed that only IL-13Rα1 was involved in both cytokine−cytokine receptor interaction and JAK−STAT signaling pathways (Fig. 6C). Further Western blot verified that IL-13Rα1 was decreased after IPA treatment both in EGCs (Fig. 6D) and the gut of PD mice (Fig. 6E), while IL-13Rα1 was overexpressed after PXR was knocked down instead of AhR inhibited in rotenone-challenged EGCs (Fig. 6D), indicating that IL-13Rα1 was in the downstream of PXR. Moreover, we found that the expression of COX-2 was decreased when IL-13Rα1 was deficient by knocking down its gene, while it could not be further decreased with additional IPA treatment (Fig. 6F), suggesting that IL-13Rα1 was necessary in IPA treatment of PD. We also found that IPA treatment decreased the production IL-13, ligand of IL-13Rα1, in rotenone-stimulated EGCs (Fig. 6G) and in the colon of PD mice (Fig. 6H), further demonstrating that IL-13Rα1 related cytokine−cytokine receptor interaction pathway was

Western blot analysis of IL-13Rα1 in the colon. (F) Western blot analysis of COX-2 after knockdown IL-13Rα1. (G) The level of IL-13 in EGCs. (H) The level of IL-13 in the colon. (I) Western blot analysis of *p*-JAK1 and JAK1 in EGCs. (J) Western blot analysis of p-STAT6 and STAT6 in EGCs. (K) Western blot analysis of *p*-JAK1 and JAK1 in the colon. (L) Western blot analysis of p-STAT6 and STAT6 in the colon. Represent images of Western blot were from 4 to 6 independent experiments. Data are presented as mean ± SEM. $^{*}P < 0.05$, $^{**}P < 0.01$, $^{***}P < 0.001$ *versus* Control cells (mice); $^{\#}P < 0.05$, $^{\#\#}P < 0.01$, $^{\#\#\#}P < 0.001$ *versus* Rotenone-challenged cells (mice).

critical in IPA regulation of EGCs. JAK1−STAT6 was reported to be the main pathway among JAK−STAT pathways that could be regulated by IL-13Rα1 signaling[25], we sought to explore its activity in IPA treated PD models. The data showed that the phosphorylation of JAK1 and STAT6 markedly reduced in both *in vitro* (Fig. 6I and J) and *in vivo* (Fig. 6K and L) PD models. When *IL-13Rα1* gene was silenced, the phosphorylation of JAK1 and STAT6 was decreased, and IPA treatment could not further suppress JAK1−STAT6 activities in the rotenone-stimulated EGCs (Fig. 6I and J), proving that JAK1−STAT6 was the downstream pathway of IL-13Rα1signaling in IPA-treated PD models.

The above results illustrated that when IPA bound to PXR in EGCs, it inhibited IL-13Rα1 involved cytokine−cytokine receptor interaction pathway, and then suppressed downstream JAK1−STAT6 signaling, thereby suppressed inflammation and improved intestinal and dopaminergic neuronal functions of PD mice through gut−brain axis.

4. Discussion

In the present work, we focused on gut−brain axis, and tried to describe the impacts of gut microbiota metabolite IPA in regulating EGCs to alleviate PD pathological damages. We identified that IPA was the important differential microbial metabolite, capable of regulating EGC function, and therefore improved intestinal and brain function of PD through gut−brain axis. And finally, we clarified that IPA bound to PXR of EGCs, inhibited IL-13Rα1 pathway and its downstream JAK1−STAT6 signaling pathway, thereby protected intestinal function, alleviated PD pathological injury, improved motor coordination of PD mice. Our present study provided novel evidence for the relationship between intestinal alterations and brain function in PD.

It was reported that EGCs could interact with microbiota and cooperate with enteric neurons to regulate ENS function[10,26]. Previous studies showed that either genetic ablation of EGCs or destructing EGC network by chemical or autoimmune T-cell-targeted led to the damage of intestinal integrity[5,26]. Moreover, in PD patients, EGC gliosis was observed in the inflammatory colon at the disease onset[27,28] and particularly GFAP was observed to be phosphorylated at the serine 13[29]. Interestingly, this phenomenon was only found in PD patients, not in multiple system atrophy or progressive supranuclear palsy, suggesting that EGC activation was closely related to PD pathological changes. Previous study in our Lab has demonstrated that inhibiting EGC gliosis in PD mice alleviated intestinal inflammation and dopaminergic neuronal function, highlighting the critical role of EGCs in spreading intestinal damage to the brain through gut−brain axis. However, there was still lack of evidence focusing on the way of regulating EGC function.

Gut microbiota interacts with EGCs and affects the survival and function of EGCs[30]. The number of EGCs significantly decreased in germ-free mice and less EGCs migrated to the lamina propria for maintaining intestinal homeostasis in the mice with gut microbiota dysbiosis[9]. Besides these studies, we found that EGCs were abnormally activated in PD mice, which was suppressed after FMT, demonstrating the importance of gut microbiota in the regulation of EGCs. The microbial metabolites build up a bridge between gut microbiota and EGCs for supporting their communication. The significant microbial metabolite that regulates EGCs probably can regress PD pathological progression. Increasing microbial metabolites are reported to be changed in PD patients and PD models in order to identify the most significant microbial metabolite which could regulate the function of EGCs, we performed metabolomics and 16S rRNA analysis. By comparing correlation coefficient between overlapped differential metabolites and differential microbiota, as well as calculating the correlation coefficient between differential metabolites and pathological indexes of PD, we identified IPA as the most affected differential metabolite that was most possible to regulate the function of EGCs. We also identified *Lachnospiraceae_UCG-006* was the most affected bacteria by correlation analysis, which was reported to be highly related to the production of IPA[20-22]. Further exploration and verification the specific relationship between *Lachnospiraceae_UCG-006* and IPA will provide more evidence to support our findings. However, this bacterium was now not commercially available and limited our further experiments.

IPA is a main indole derivative of gut microbiota produced in tryptophan metabolism[31], predominantly exerting anti-inflammatory effect. It has been reported that IPA could relieve doxorubicin-induced cardiomyocyte inflammation[32] and suppress indoxyl sulfate-induced expression of inflammatory genes in proximal tubular cells[33]. Besides, a metabolomics analysis was reported that IPA decreased in the serum of PD patient[34], suggesting that IPA could be the potential biomarker of PD. However, there was not much evidence indicating the effect of IPA on neuropathological damage in PD. More importantly, IPA could directly reduce astrocyte gliosis and inhibit their secretion of inflammatory factors *in vitro*[35]. As having the similar profiles of astrocytes, EGCs were also found to be regulated by IPA in this study, showing that IPA could inhibit the reactive EGC gliosis as well as its mediated inflammation. Of note, we uncovered that IPA mainly bound to PXR of EGCs, rather than other cells in the intestine, to exert therapeutic effects on alleviating PD pathologic damage. Moreover, IPA has been reported in various animal models to reduce intestinal barrier permeability, promote the expression of intestinal barrier tight proteins, and effectively alleviate intestinal inflammation[36-38]. Consistent with these studies, our data on PD mice demonstrated that IPA could alleviate gut dysfunction, including intestinal inflammation, gut barrier damage and intestinal peristalsis, and the function of IPA were achieved *via* suppressing EGC gliosis. Interestingly, we also found that IPA could conversely alleviate gut dysbiosis in PD mice, indicating that IPA probably had mutual regulation with gut microbiota, which need further investigation in the future.

IPA was reported to exert pharmacological effects, mainly depending on the interactions with PXR and AhR. Here we figured out IPA dominantly interacted with PXR to exert the therapeutic effect on restoring EGC function. More in depth, by employing transcriptomics analysis, we identified *IL-13Rα1* was the most affected genes and the downstream protein of PXR by IPA treatment, which was involved in both cytokine−cytokine receptor interaction and JAK−STAT signaling pathways. IL-13Rα1 is a ligand binding subunit and forms receptor heterodimerization with IL-4 receptor to have high affinity for IL-13[39], belonging to cytokine−cytokine receptor interaction pathway. Cytokine−cytokine receptor interactions play an important role in immunological and inflammatory responses in diseases, involving signaling homology, convergence of signaling pathways, and/or positive or negative feedbacks within and among cytokine systems[40]. In our study, IPA decreased IL-13Rα1 signaling, a type of cytokine−cytokine receptor interaction pathway, by reducing the level of IL-13 and expression of IL-13Rα1 in EGCs. JAK−STAT is a complex signaling pathway, including

four members of the JAK family and seven STATs[41]. Different JAKs and STATs are recruited based on their tissue specificity and the receptors engaged in the signaling event[41]. It was reported that JAK1/STAT6 was the classical downstream signaling pathway of IL-13/IL-13Rα1[42]. Once IL-13 binds to IL-13Rα1, JAK1 associated with the cytoplasmic tails of the receptors are activated, and phosphorylate conserved tyrosine residues on the receptor. This phosphorylation leads to the binding of the cytoplasmic STAT6 by its Src homology-2 domain to the phosphorylated receptor and then STAT6 was phosphorylated[42]. Consistent with previous study, we revealed that IL-13/IL-13Rα1 signaling was up-stream of JAK1−STAT6 pathway in EGCs treated with IPA, and the phosphorylated JAK1 and STAT6 were decreased after IPA treatment, indicating that JAK1−STAT6 signaling pathway was inhibited after IPA treatment in PD mice. Although our study illustrated the mechanisms of IPA in regulation of EGC function, the detailed mechanism of how IPA affected PXR/IL-13Rα1/JAK1−STAT6 pathway still need further experiments to clarify.

5. Conclusions

Our study illustrated that EGC gliosis might be the main peripheral pathological changes at the early stage of PD and played critical roles in spreading intestinal pathology to brain. Our data also revealed that microbial metabolite IPA inhibited EGC activation by targeting PXR, through suppressing IL-13Rα1/JAK1−STAT6 signaling pathway, and therefore alleviated neuropathological damages of PD through gut−brain axis. The present results provided evidence for early treatment of PD by targeting EGCs and promoting microbial metabolite IPA production.

Acknowledgments

This work was financially supported by the National Key Research and Development Program of China (No.2024YFA0919900); the National Natural Science Foundation of Beijing (No. L246065, China); the CAMS Innovation Found for Medical Sciences (No. 2023-I2M-2-006, China).

Author contributions

Meiyu Shang: Writing − original draft, Data curation, Conceptualization. Jingwen Ning: Investigation. Caixia Zang: Investigation. Jingwei Ma: Investigation. Yang Yang: Investigation, Formal analysis. Zhirong Wan: Investigation. Jing Zhao: Investigation. Yueqi Jiang: Investigation. Qiuzhu Chen: Investigation. Yirong Dong: Investigation. Jinrong Wang: Investigation. Fangfang Li: Investigation. Xiuqi Bao: Writing − review & editing, Validation, Supervision, Conceptualization. Dan Zhang: Writing − review & editing, Funding acquisition, Conceptualization.

Conflicts of interest

The authors declare that they have no competing interests.

Appendix A. Supporting information

Supporting information to this article can be found online at https://doi.org/10.1016/j.apsb.2025.02.029.

References

1. Hindle JV. Ageing, neurodegeneration and Parkinson's disease. *Age ageing* 2010;**39**:156−61.
2. Huang Y, Liao J, Liu X, Zhong Y, Cai X, Long L. The role of intestinal dysbiosis in Parkinson's disease. *Front Cell Infect Microbiol* 2021;**11**: 615075.
3. Hirayama M, Nishiwaki H, Hamaguchi T, Ohno K. Gastrointestinal disorders in Parkinson's disease and other Lewy body diseases. *NPJ Parkinsons Dis* 2023;**9**:71.
4. Neunlist M, Rolli Derkinderen M, Latorre R, Van Landeghem L, Coron E, Derkinderen P, et al. Enteric glial cells: recent developments and future directions. *Gastroenterology* 2014;**147**:1230−7.
5. Yu YB, Li YQ. Enteric glial cells and their role in the intestinal epithelial barrier. *World J Gastroenterol* 2014;**20**:11273.
6. Li N, Xu J, Gao H, Zhang Y, Li Y, Chang H, et al. Effect of reactive EGCs on intestinal motility and enteric neurons during endotoxemia. *J Mol Neurosci* 2022;**72**:1831−45.
7. Devos D, Lebouvier T, Lardeux B, Biraud M, Rouaud T, Pouclet H, et al. Colonic inflammation in Parkinson's disease. *Neurobiol Dis* 2013;**50**:42−8.
8. Anwar H, Iftikhar A, Muzaffar H, Almatroudi A, Allemailem KS, Navaid S, et al. Biodiversity of gut microbiota: impact of various host and environmental factors. *BioMed Res Int* 2021;**2021**:5575245.
9. Luo S, Zhu H, Zhang J, Wan D. The pivotal role of microbiota in modulating the neuronal−glial−epithelial unit. *Infect Drug Resist* 2021;**14**:5613−28.
10. Kabouridis PS, Lasrado R, McCallum S, Chng SH, Snippert HJ, Clevers H, et al. The gut microbiota keeps enteric glial cells on the move; prospective roles of the gut epithelium and immune system. *Gut Microbes* 2015;**6**:398−403.
11. Wang Q, Luo Y, Ray Chaudhuri K, Reynolds R, Tan EK, Pettersson S. The role of gut dysbiosis in Parkinson's disease: mechanistic insights and therapeutic options. *Brain* 2021;**144**:2571−93.
12. Sun MF, Shen YQ. Dysbiosis of gut microbiota and microbial metabolites in Parkinson's disease. *Ageing Res Rev* 2018;**45**:53−61.
13. Zhao Z, Ning J, Bao XQ, Shang M, Ma J, Li G, et al. Fecal microbiota transplantation protects rotenone-induced Parkinson's disease mice *via* suppressing inflammation mediated by the lipopolysaccharide-TLR4 signaling pathway through the microbiota−gut−brain axis. *Microbiome* 2021;**9**:226.
14. Shang J, Ma S, Zang C, Bao X, Wang Y, Zhang D. Gut microbiota mediates the absorption of FLZ, a new drug for Parkinson's disease treatment. *Acta Pharm Sin B* 2021;**11**:1213−26.
15. Bao XQ, Wu LY, Wang XL, Sun H, Zhang D. Squamosamide derivative FLZ protected tyrosine hydroxylase function in a chronic MPTP/probenecid mouse model of Parkinson's disease. *Naunyn Schmiedebergs Arch Pharmacol* 2015;**388**:549−56.
16. Zhao Z, Li F, Ning J, Peng R, Shang J, Liu H, et al. Novel compound FLZ alleviates rotenone-induced PD mouse model by suppressing TLR4/MyD88/NF-κB pathway through microbiota−gut−brain axis. *Acta Pharm Sin B* 2021;**11**:2859−79.
17. Bao XQ, Wang XL, Zhang D. FLZ attenuates α-synuclein-induced neurotoxicity by activating heat shock protein 70. *Mol Neurobiol* 2017;**54**:349−61.
18. Zhao Z, Bao XQ, Zhang Z, Liu H, Zhang D. Phloroglucinol derivative compound 21 attenuates cuprizone-induced multiple sclerosis mice through promoting remyelination and inhibiting neuroinflammation. *Sci China Life Sci* 2020;**63**:905−14.
19. Benvenuti L, D'Antongiovanni V, Pellegrini C, Antonioli L, Bernardini N, Blandizzi C, et al. Enteric glia at the crossroads between intestinal immune system and epithelial barrier: implications for Parkinson disease. *Int J Mol Sci* 2020;**21**:9199.
20. Ahmad MI, Ijaz MU, Hussain M, Haq Iu, Zhao D, Li C. High-fat proteins drive dynamic changes in gut microbiota, hepatic metabolome, and endotoxemia−TLR-4−NFκB-mediated inflammation in mice. *J Agric Food Chem* 2020;**68**:11710−25.

21. Cheng H, Liu J, Zhang D, Wang J, Tan Y, Feng W, et al. Ginsenoside Rg1 alleviates acute ulcerative colitis by modulating gut microbiota and microbial tryptophan metabolism. *Front Immunol* 2022;**13**:817600.
22. Zhang Y, Yao W, Zhang W, Wen Y, Hua Y, Ji P, et al. Yujin powder improves large intestine dampness−heat syndrome by regulating gut microbiota and serum metabolism. *Biomed Chromatogr* 2023;**37**:e5719.
23. Granados JC, Falah K, Koo I, Morgan EW, Perdew GH, Patterson AD, et al. AHR is a master regulator of diverse pathways in endogenous metabolism. *Sci Rep* 2022;**12**:16625.
24. Illés P, Krasulová K, Vyhlídalová B, Poulíková K, Marcalíková A, Pečinková P, et al. Indole microbial intestinal metabolites expand the repertoire of ligands and agonists of the human pregnane X receptor. *Toxicol Lett* 2020;**334**:87−93.
25. Hershey GKK. IL-13 receptors and signaling pathways: an evolving web. *J Allergy Clin Immunol* 2003;**111**:677−90.
26. Li S, Zhao L, Xiao J, Guo Y, Fu R, Zhang Y, et al. The gut microbiome: an important role in neurodegenerative diseases and their therapeutic advances. *Mol Cell Biochem* 2023;**479**:2217−43.
27. Montalbán Rodríguez A, Abalo R, López Gómez L. From the gut to the brain: the role of enteric glial cells and their involvement in the pathogenesis of Parkinson's disease. *Int J Mol Sci* 2024;**25**:1294.
28. Ochoa Cortes F, Turco F, Linan Rico A, Soghomonyan S, Whitaker E, Wehner S, et al. Enteric glial cells: a new frontier in neurogastroenterology and clinical target for inflammatory bowel diseases. *Inflamm Bowel Dis* 2016;**22**:433−49.
29. Clairembault T, Kamphuis W, Leclair Visonneau L, Rolli Derkinderen M, Coron E, Neunlist M, et al. Enteric GFAP expression and phosphorylation in Parkinson's disease. *J Neurochem* 2014;**130**:805−15.
30. Pellegrini C, Antonioli L, Colucci R, Blandizzi C, Fornai M. Interplay among gut microbiota, intestinal mucosal barrier and enteric neuroimmune system: a common path to neurodegenerative diseases?. *Acta Neuropathol* 2018;**136**:345−61.
31. Zhang J, Zhu S, Ma N, Johnston LJ, Wu C, Ma X. Metabolites of microbiota response to tryptophan and intestinal mucosal immunity: a therapeutic target to control intestinal inflammation. *Med Res Rev* 2021;**41**:1061−88.
32. Li C, Chang J, Wang Y, Pan G. Indole-3-propionic acid, a product of intestinal flora, inhibits the HDAC6/NOX2 signaling and relieves doxorubicin-induced cardiomyocyte damage. *Folia Morphol* 2024;**83**:382−90.
33. Yisireyili M, Takeshita K, Saito S, Murohara T, Niwa T. Indole-3-propionic acid suppresses indoxyl sulfate-induced expression of fibrotic and inflammatory genes in proximal tubular cells. *Nagoya J Med Sci* 2017;**79**:477.
34. Luan H, Wang X, Cai Z. Mass spectrometry-based metabolomics: targeting the crosstalk between gut microbiota and brain in neurodegenerative disorders. *Mass Spectrom Rev* 2019;**38**:22−33.
35. Garcez ML, Tan VX, Heng B, Guillemin GJ. Sodium butyrate and indole-3-propionic acid prevent the increase of cytokines and kynurenine levels in LPS-induced human primary astrocytes. *Int J Tryptophan Res* 2020;**13**:1178646920978404.
36. Li J, Zhang L, Wu T, Li Y, Zhou X, Ruan Z. Indole-3-propionic acid improved the intestinal barrier by enhancing epithelial barrier and mucus barrier. *J Agric Food Chem* 2020;**69**:1487−95.
37. Jennis M, Cavanaugh C, Leo G, Mabus J, Lenhard J, Hornby P. *Microbiota-derived tryptophan indoles increase after gastric bypass surgery and reduce intestinal permeability in vitro and in vivo. Neurogastroenterol Motil*, vol. 30; 2018. p. e13178.
38. Ismael S, Rodrigues C, Santos GM, Castela I, Barreiros Mota I, Almeida MJ, et al. IPA and its precursors differently modulate the proliferation, differentiation, and integrity of intestinal epithelial cells. *Nutr Res Pract* 2023;**17**:616.
39. Kelly Welch A, Hanson EM, Keegan AD. Interleukin-13 (IL-13) pathway. *Sci STKE* 2005;**2005**:cm8.
40. Turrin NP, Plata Salamán CR. Cytokine−cytokine interactions and the brain. *Brain Res Bull* 2000;**51**:3−9.
41. Imada K, Leonard WJ. The JAK−STAT pathway. *Mol Immunol* 2000;**37**:1−11.
42. Karpathiou G, Papoudou Bai A, Ferrand E, Dumollard JM, Peoc'h M. STAT6: a review of a signaling pathway implicated in various diseases with a special emphasis in its usefulness in pathology. *Pathol Res Pract* 2021;**223**:153477.